CERN-ACC-NOTE

16 October 2018
patricia.ribes.metidieri@cern.ch
christina.yin.vallgren@cern.ch

TDIS pressure profile simulations after LS2

P. Ribes Metidieri, C. Yin Vallgren, G. Skripka, G. Iadarola, G. Bregliozzi
CERN, CH-1211 Geneva, Switzerland

Keywords: LS2, TDIS, electron cloud, dynamic pressure profile, VASCO

Summary

During the LS2 (Long Shutdown 2), the current TDI (Beam Absorber for Injection) will be replaced by the new so called, TDIS (Beam Absorber for Injection Segmented). A throughout static/dynamic pressure profile validation in the concerned sectors is important for the upcoming beam operations. This document summarizes the outcome of the TDIS pressure profile simulations.

Contents

1 Introduction

During the LS2 (Long Shutdown 2), the new TDIS will replace the current TDI in both Long Straight Section (LSS) 2 and LSS8 injection regions. The TDIS plays an important role in the protection of the downstream equipment in the LHC injection regions in case of malfunctioning of the MKI injection kickers, and it is equipped with movable jaws [1].

The replacement has an impact on the vacuum layout. In this document, a detailed study on vacuum profile simulations is presented in order to understand its vacuum performance during beam operation after the LS2. Since the ALICE experiment is very sensitive to the high pressure in the LSS region, in this document, we chose to mainly focus on the simulations applied for the TDIS that will be installed in the LSS2. Because of the symmetry in the LHC layout, the same simulation results are valid for the TDIS in the LSS8. All the simulations in this report are focused on an unrealistic scenario with high intensity beams with nominal beam parameters immediately after the LS2. This is due to the incertitude of the possible used strategy during the commissioning period after the LS2 and the difficulties to have detailed simulation of electron flux as a function of different SEY values and different filling scheme. This study is very important to determine a possible materials and coating configuration for the TDIS that would full immediately the vacuum requirements imposed by the ALICE experiment and the LHC machine.

2 TDIS Layout

Figure 1 (top) shows the current layout in the region of TDI whilst Fig. 1 (bottom) shows the future layout in the region of TDIS after LS2 [2]. The total length of the TDIS is 5740 mm with three separated tanks, including two additional sector valves on both extremities. The reason of having two additional sector valves is to make it possible for the in-lab in-situ bake-out on surface and later a safe transport and installation in the tunnel. The three tanks contain the so-called RF shield, made of stainless steel, as illustrated in Fig. 2. The first two tanks are equipped with absorbing jaws made of graphite SGL7550 [3] vacuum fired at 950 °C for 6 hours while the jaw in the last tank is combined of 965 mm long Ti_6Al_4V block and a 600 mm long CuCrZr block.

Each tank of the TDIS will be equipped with two ion pumps (Agilent Vaclon Plus 75 [4]) on the top and two NEG cartridges (CapaciTorr HV2100 with NUDE configuration [5]) at the bottom, as illustrated in Fig. 3.

3 Pressure simulation approach using VASCO

VASCO (VAcuum Stability COde) is a code integrally developed at CERN for the simulation of the pressure profile in a cylindrical geometry considering beam induced effects [6]. In order to optimize the performance of the code for large geometries, VASCO was rewritten in Python in Ref. [7], under the name of PyVASCO (VAcuum Stability COde written in Python), and it has recently been modified in order to extend its functionality.

Some of the included modifications allow simulating the dynamic pressure by using an interpolated ESD (Electron Stimulated Desorption) and SEY (Secondary Electron Yield) for

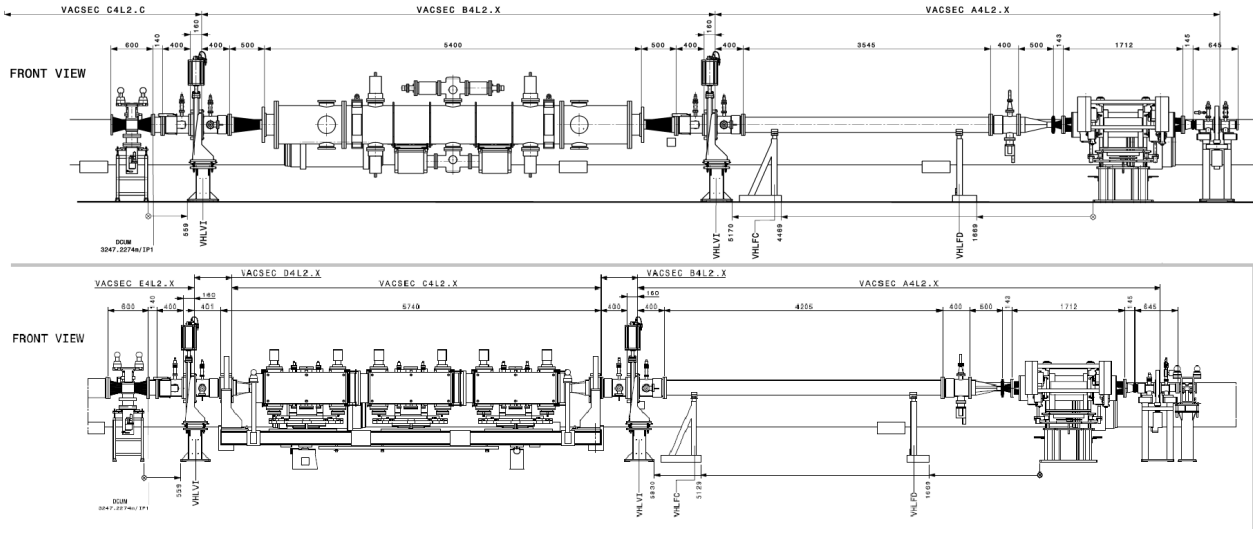

Figure 1: Side view of the current layout (top figure) and of the proposed layout for after LS2 (bottom figure) in sector A4L2.

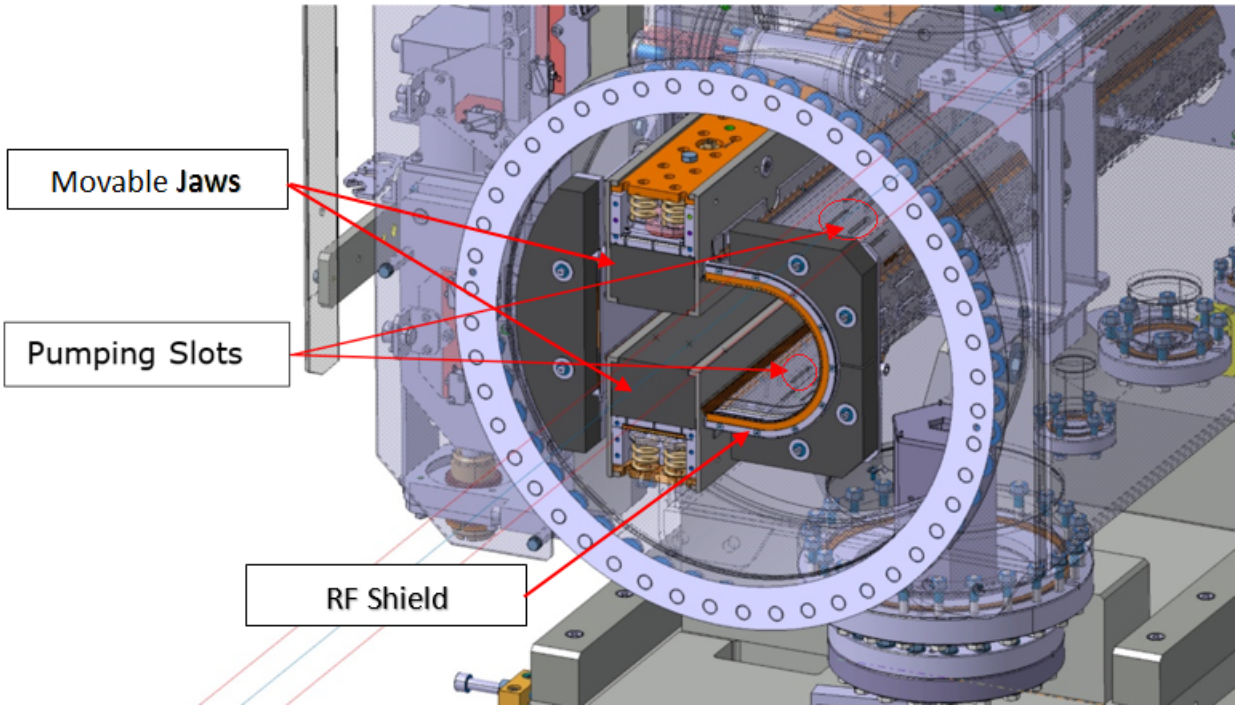

Figure 2: Mechanical drawing of an opened TDIS tank.

each of the materials introduced in the simulation, for a given (homogeneous) accumulated electron dose on the walls. Also, it has been extended for simulations of the pressure evolution for different assumed electron doses (conditioning effect) and simulations of the maximum pressure rise as a function of the half-gap in the TDIS.

PyVASCO has been used to estimate both the static pressure profile and the dynamic pressure profile in the TDIS region after the LS2. The layout used for the simulation is

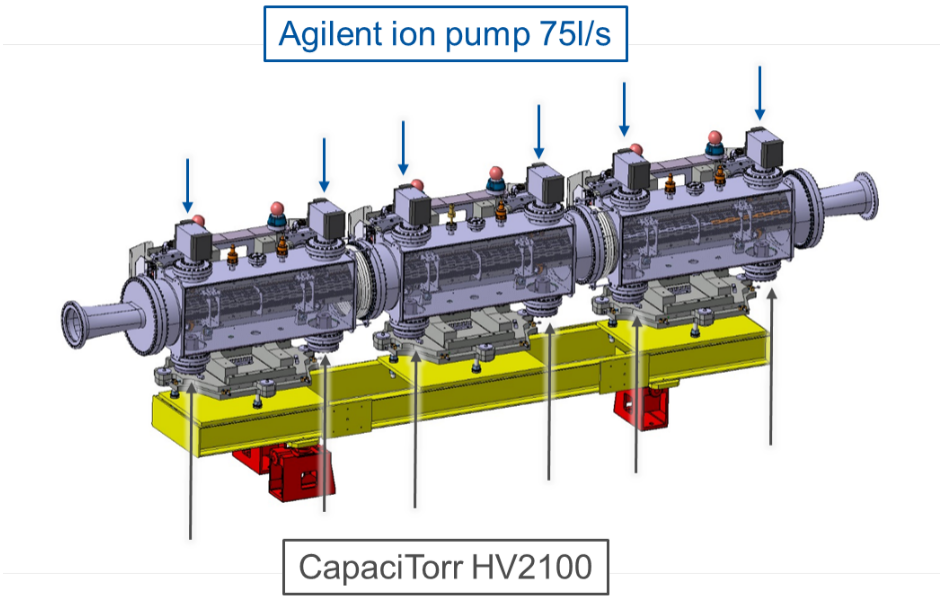

Figure 3: 3D model of the three TDIS tanks, each equipped with two ion pumps on the top and two NEG cartridges at the bottom of the tank.

shown in Fig. 4.

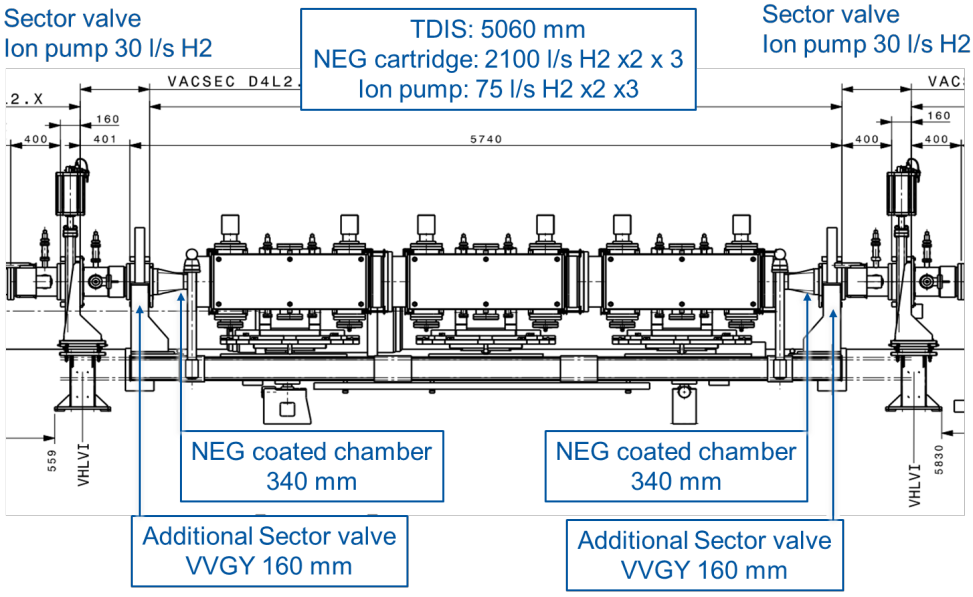

Figure 4: Schematic layout for PyVASCO simulations.

PyVASCO treats the vacuum beam pipes as one-dimensional tubes, assuming radial symmetry with cylindrical conductance and homogeneous photon and electron fluxes. A block diagram of the TDIS geometry as treated by PyVASCO is depicted in Fig. 5. In order to account for the non-symmetry of the TDIS tanks and the mobility of the jaws, the conductance of the tanks for different jaw openings has been estimated using Molflow+, a

software based on Monte-Carlo simulations in static ultra high vacuum (UHV) [8]. Then, the estimated conductance for different half-gaps has been used to compute the equivalent diameter of a cylindrical tube of the same length as the TDIS tank and with the same conductance, as presented in Fig. 6 .

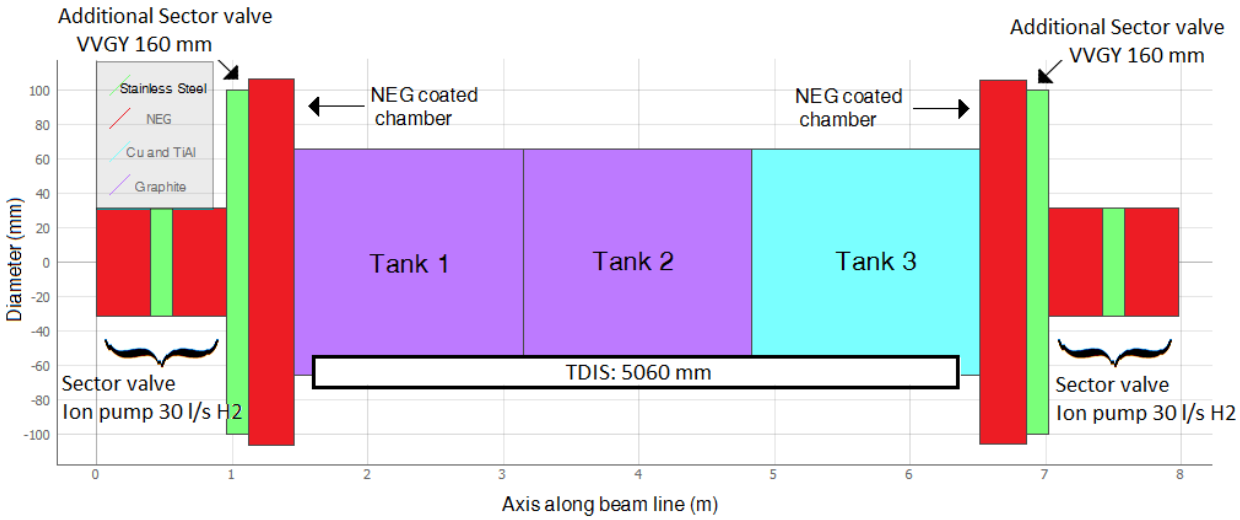

Figure 5: Vacuum chamber configuration presented in block diagram used for PyVASCO simulations.

The total nominal pumping speed for each of the considered gases for the TDIS tanks is presented in Tab. 1. Since the pumping speed of the ion pump strongly depends on the base pressure in the system, in the simulations an optimal operation pressure of 10^{-7} mbar is assumed to simplify the calculations.

However, since most of the pumping will occur through the pumping slots in the RF shield (see Fig. 2), the pumps will generate an effective distributed pumping speed inside the TDIS tanks. This effective distributed pumping speed has been evaluated in a dedicated Molflow+ model (Fig. 7). The obtained pumping speeds for different gases at the half-gap of 26 mm are presented in Tab. 1. Since the original Molflow+ model was built with 26 mm half gap and modifying the geometry at this point would have been extremely time-consuming, the effective distributed pumping was computed for this particular half-gap and the results presented in Tab. 1 are still valid for other half-gaps given that most of the pumping occurs through the RF shield slots.

4 Static pressure profile

4.1 Thermal outgassing rate for different surfaces

The static pressure profile is dominated by the thermal outgassing of the chamber surfaces. The measures of the total outgassing for the TDI in Refs. [tdi1,tdi2] has been used as a reference to estimate the total outgassing in the future TDIS. Then, the total outgassing has been scaled to an outgassing per unit area in the simplified geometry used in PyVASCO. The scaled outgassing rate used as an input for PyVASCO is listed in Tab. 2.

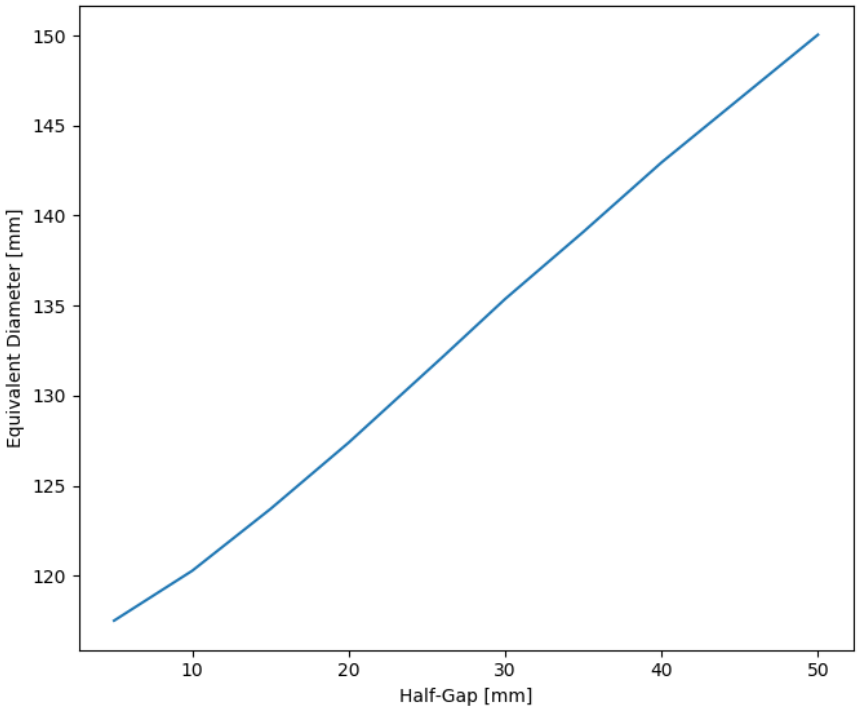

Figure 6: Computed equivalent diameter of a cylindrical tube to be used in PyVASCO simulations as a function of the half-gap.

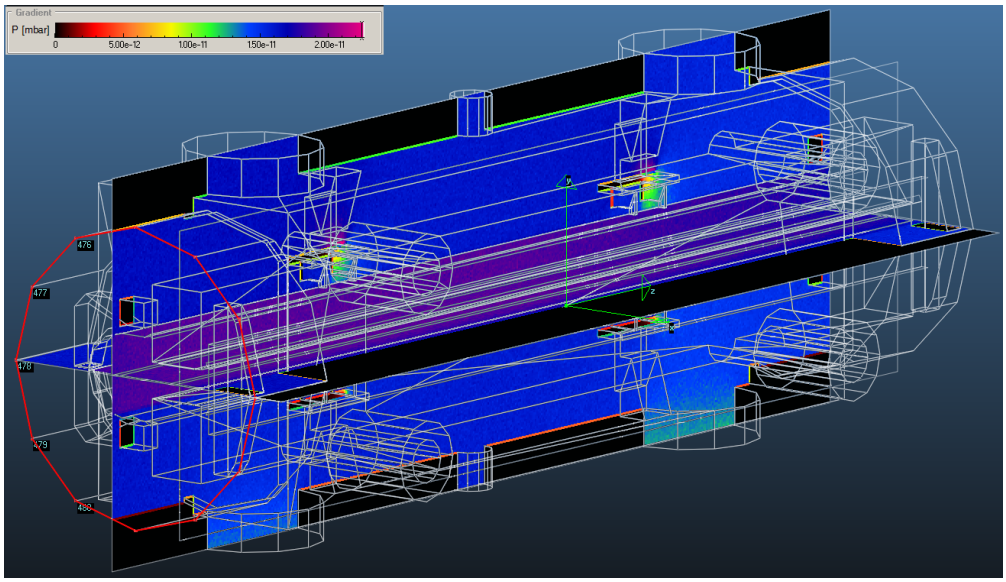

Figure 7: Molflow+ model of one of the TDIS tanks with a half-gap of 26 mm.

No NEG coated parts have been considered in the warm modules, and the NEG coated chambers adjacent to the TDIS tanks are considered to pump at the nominal pumping speed

Table 1: Nominal values of pumping speed for the Agilent ion pumps (at an optimal operation pressure of 10^{-7} mbar*) and CapaciTorr HV2100, and effective distributed pumping speed

	Agilent Valcon Ion pump 75 l/s* l/s	CapaciTorr HV2100 l/s	Effective distributed pumping speed over one tank at 26 mm half-gap l/s
H_2	75	2100	3377
CH_4	60	0	118
CO/CO_2	65	625	1036

of NEG after vacuum activation.

Table 2: Scaled thermal outgassing rate for the TDIS tanks applied in the PyVASCO simulations.

	Q_{H_2} $\frac{\text{mbar l}}{\text{s cm}^2}$	Q_{CH_4} $\frac{\text{mbar l}}{\text{s cm}^2}$	Q_{CO} $\frac{\text{mbar l}}{\text{s cm}^2}$	Q_{CO_2} $\frac{\text{mbar l}}{\text{s cm}^2}$	Q_{Total} $\frac{\text{mbar l}}{\text{s cm}^2}$
TDIS tank	1.0×10^{-11}	2.5×10^{-14}	1.5×10^{-13}	3.0×10^{-14}	1.0×10^{-11}

4.2 Static pressure profile results

Substituting the real geometry by that of an equivalent cylinder in order to compute the total outgassing of a given component proves to be a good approach for a great part of the components in an accelerator, and the error introduced by doing so is, generally, negligible. However, this is not the case for the TDIS tanks, since the equivalent conductance for these pieces mainly consists in that of the aperture between the jaws and the RF shield, and the outgassing surface is much bigger than that of the computed equivalent cylinder. In order to solve this problem, the total outgassing surface of the TDIS tanks have been estimated based on the measurements on the current TDI [9, 10].

The result of the simulation of the static pressure profile in the TDIS is presented in Fig. 8. Based on the presented geometry and degassing rates for the different parts of the TDIS, it can be observed that the pressure distribution is dominated by H_2 gas. The total pressure (N_2 equivalent for a Bayard-Alpert ionization gauge) reaches a maximum value of 1.1×10^{-10} mbar in the middle of the geometry.

5 Dynamic pressure profile

Estimating the dynamic pressure profile is considerably more complicated due to the beam induced effects, namely, the build-up of electron cloud, gas ionization due to the interactions of the beam with the residual gases, the impingement of synchrotron radiation on the surface of the vacuum chambers, etc.

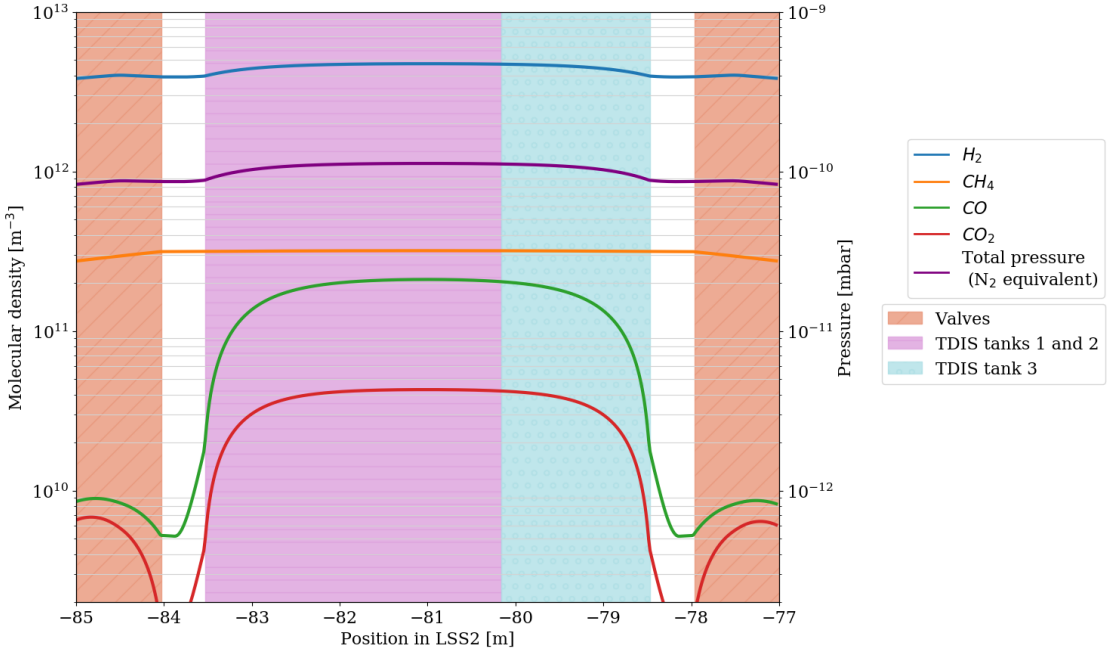

Figure 8: Simulated static pressure profile in the TDIS for a half-gap of 25 mm.

According to the synchrotron radiation simulations presented in Ref. [11], the expected synchrotron radiation in the area of the TDIS is negligible, and the build-up of electron cloud in the TDIS region is considered to be the main contribution to the dynamic pressure rise.

For this reason, special attention has been given to the simulation of the electron cloud build-up in the TDIS [12], in order to give an accurate estimation of the electron flux impinging the surface of the vacuum chambers. It is also important to mention that the dynamic pressure profile simulations for the TDIS are mainly focused in the commissioning of the machine after LS2, since it is during this period that the dynamical pressure rise in the TDIS is foreseen to be the highest, and therefore, the most critical for the operation of the machine.

The commissioning period after the LS2 will consist of several months of a gentle rise in bunch number and population, which will give the jaws and the RF shields time to receive an important amount of electrons before starting with nominal LIU beams. In this time, the ESD and the SEY in the tanks would have decreased significantly with respect to the values of the unscrubbed materials.

However, it is not straightforward to estimate precisely the ESD and SEY in the tanks by the time when high intensity beams start running in the machine. Due to these difficulties, this study has been carried out considering the unrealistic scenario of a short or non-existing conditioning period, immediately followed by high intensity beams with the nominal beam parameters, listed in Tab. 3.

Thus, in this scenario, the expected SEY and ESD yield of the different parts of the TDIS after in-lab bake-out and installation will be the maximum possible for the corresponding materials. In all the presented simulations, it has been assumed that ESD curve of baked copper (shown in Fig. 9) is, essentially, the same as for stainless steel after bake-out and that

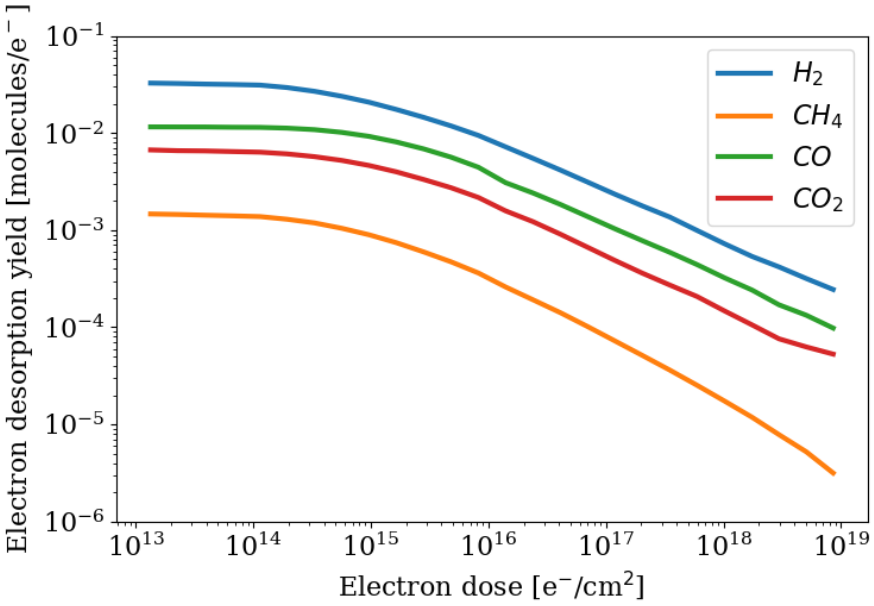

Figure 9: ESD curve as a function of electron dose for copper after a 24 hours bake-out at 250 ° C.[13]

the main contribution of desorbed molecules comes from the RF Shield (made of stainless steel) in all three TDIS tanks. In all simulations the ESD yield for the different gas species has been considered constant.

Table 3: Nominal beam parameters for the LHC after LS2

Beam energy [GeV]	450
Beam intensity [p/bunch]	2.2×10^{11}
$N_{bunches}$	2748
Bunch length [ns]	1.2
Beam current [A]	1.13
Bunch spacing [ns]	25

5.1 Case studies

In order to understand the role of different materials and surface coatings in the TDIS tanks in the suppression of the electron cloud and, consequently, in the reduction of the dynamic pressure rise, four different cases have been studied. The surface properties used for each of the cases are presented in Tab. 4 and in Fig. 10.

Case 1 studies the dynamic pressure in the TDIS baseline design, without coatings. From the point of view of electron cloud build-up, this is the worst case among the studied scenarios. In cases 2, 3 and 4, the effects of coating the jaws of the third tank, or/and the RF Shield along the three tanks with a-C coating (with SEY 1.0) are considered, respectively.

	Case 1		Case 2		Case 3		Case 4	
	Tanks 1 and 2	Tank 3	Tanks 1 and 2	Tank 3	Tanks 1 and 2	Tank 3	Tanks 1 and 2	Tank 3
Jaws	Graphite SEY = 1.0	Ti_6Al_4V and CuCrZr SEY = 1.6	Graphite SEY = 1.0	a-C coating[a] SEY = 1.0	Graphite SEY = 1.0	Ti_6Al_4V and CuCrZr SEY = 1.6	Graphite SEY = 1.0	a-C coating SEY = 1.0
RF Shield	Stainless Steel SEY = 1.6	Stainless Steel SEY = 1.6	Stainless Steel SEY = 1.6	Stainless Steel SEY = 1.6	a-C coating SEY = 1.0	a-C coating SEY = 1.0	a-C coating SEY = 1.0	a-C coating SEY = 1.0
Sides of jaws	Stainless Steel SEY = 1.6							
Back plate	Stainless Steel SEY = 1.6							

Table 4: Materials and coating used for the jaws and RF-shield in the TDIS tanks for the four cases studied in the simulations of dynamic pressure rise.

[a] a-C stands for amorphous carbon

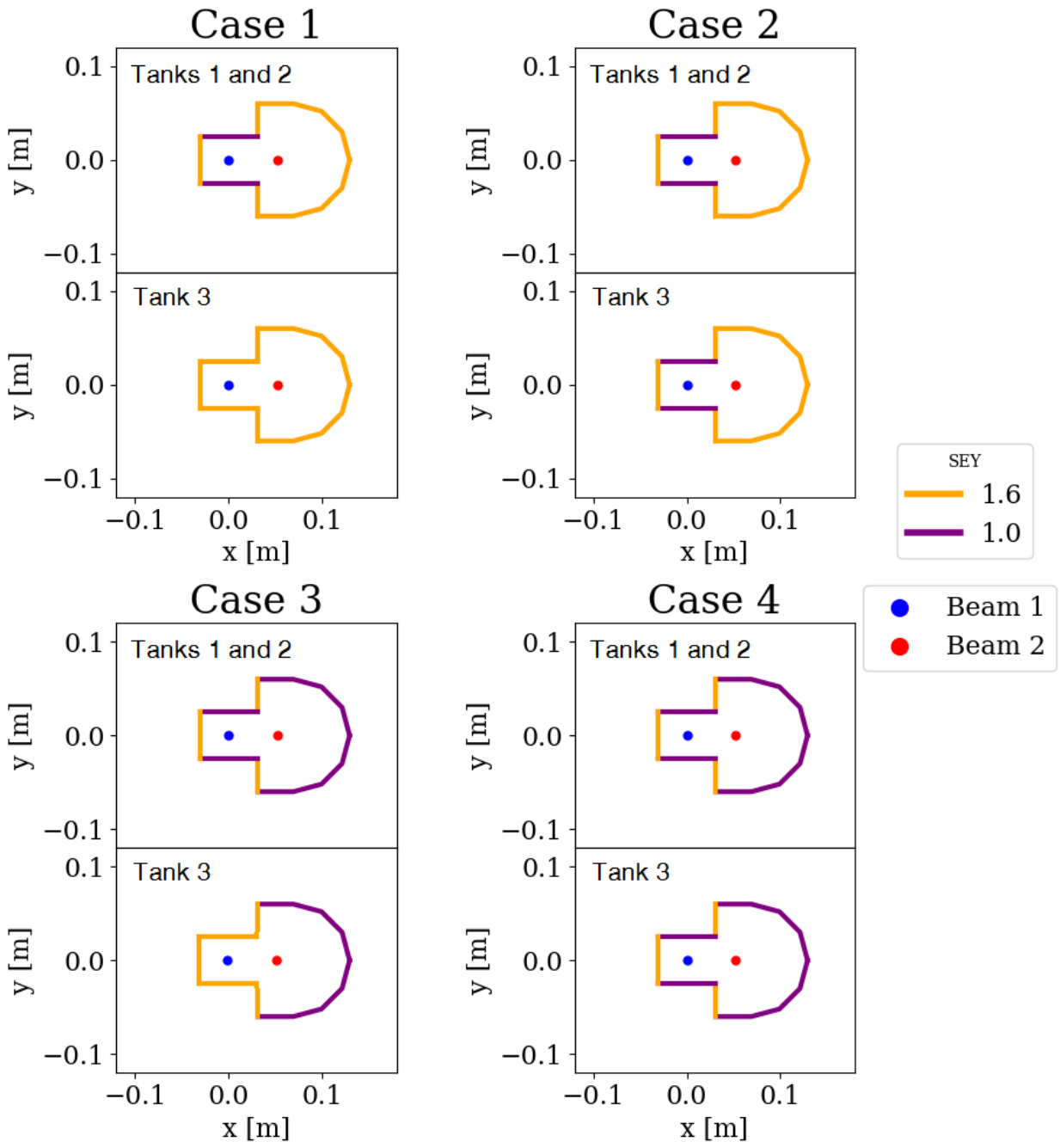

Figure 10: Distribution of the SEY for all the studied cases and half-gap of 25 mm.

5.2 Electron flux

Electron cloud build-up in the TDIS was simulated with PyECLOUD [14] depending on the position of absorbing jaws and SEY distribution corresponding to the cases shown in Fig. 10. The two counter-rotating beams share the same chamber in the TDIS and the dynamics of the electrons gets more complicated due to the hybrid bunch spacing along the device. To correctly model the presence of two beams we take into account their different arrival times

and variations of the transverse sizes. More details about the simulations for the formation of electron cloud in the TDIS area can be founf in Ref. [12].

PyECLOUD simulations have shown that the electron accumulation in TDIS strongly depends on the location along the device and the half-gap [15]. However, even though the electron current inside the TDIS is not homogeneous, only the total electron current on the surface has been considered as an input for PyVASCO.

Figure 11a shows the total electron current versus the half-gap in tanks one and two for different cases of SEY distribution. In cases 3 and 4 when the RF shield is coated with a-C (SEY 1.0) the electron current in tanks one and two becomes negligible.

Figure 11b shows the total electron current versus the half-gap in tank three for different cases of SEY distribution. Again, simulations for cases 3 and 4 with coated RF shield show significantly smaller electron currents, and no multipacting happening up to half-gaps of 15 mm in case 3.

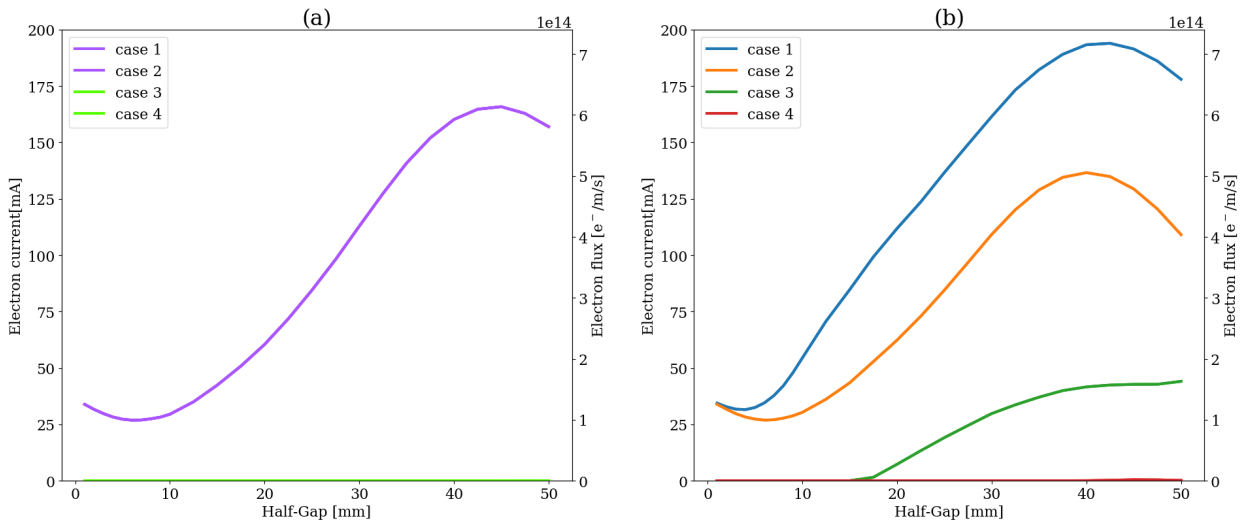

Figure 11: Electron current as a function of the half-gap in (a) the first and second TDIS tanks and (b) in the third TDIS tank, for the different cases considered.

5.3 Results and comparison

Figures 12, 13, 14 and 15 show a comparison of the dynamic density profile in the region of the TDIS for the different studied cases , at half-gaps of 4 mm, 25 mm, 45 mm and 50 mm, respectively. The 45 mm half-gap case is shown since the electron current due to electron cloud is maximum at this aperture, as presented in Fig. 11.

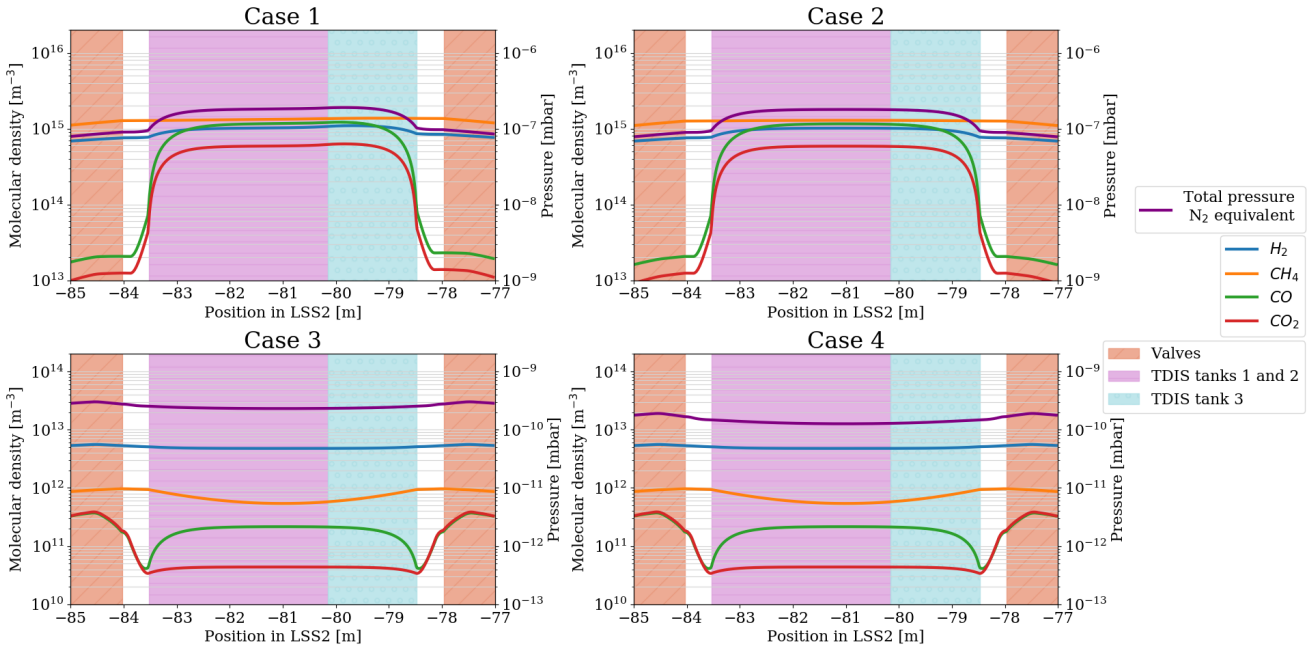

Figure 12: Dynamic density profiles for the different studied cases at a half-gap of 4 mm. The total pressure in N_2 equivalent for a Bayard-Alpert ionization gauge is also shown.

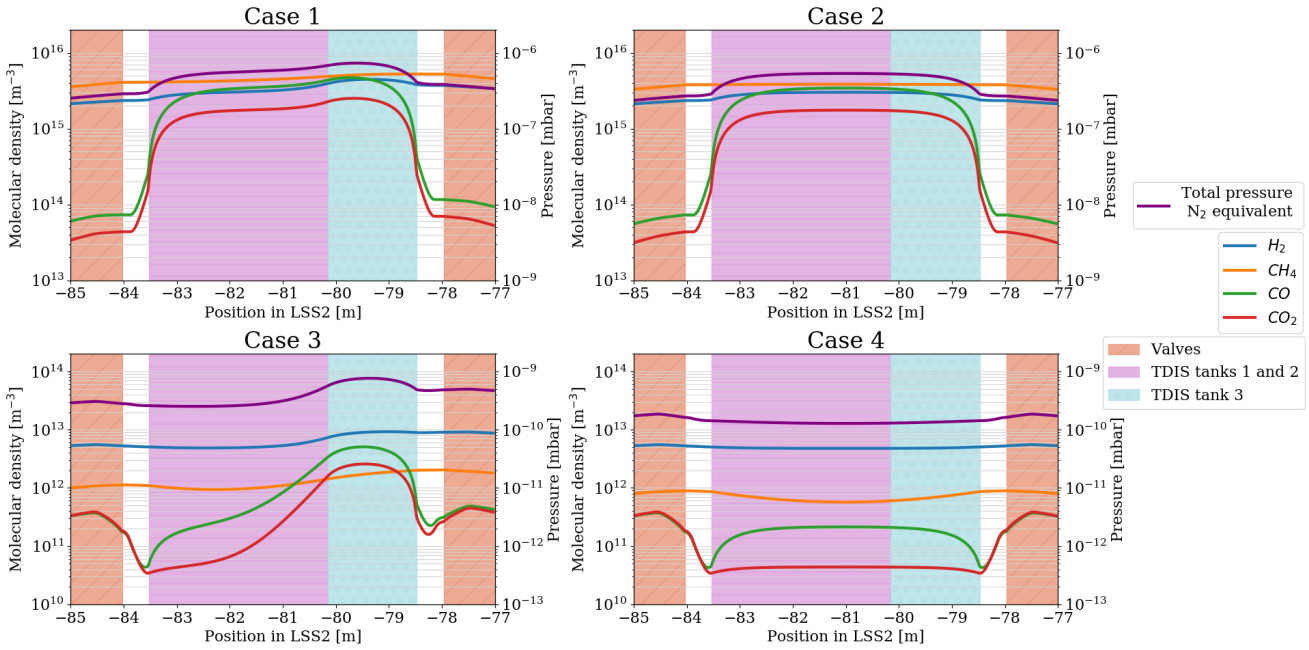

Figure 13: Dynamic density profiles for the different studied cases at a half-gap of 25 mm. The total pressure in N_2 equivalent for a Bayard-Alpert ionization gauge is also shown.

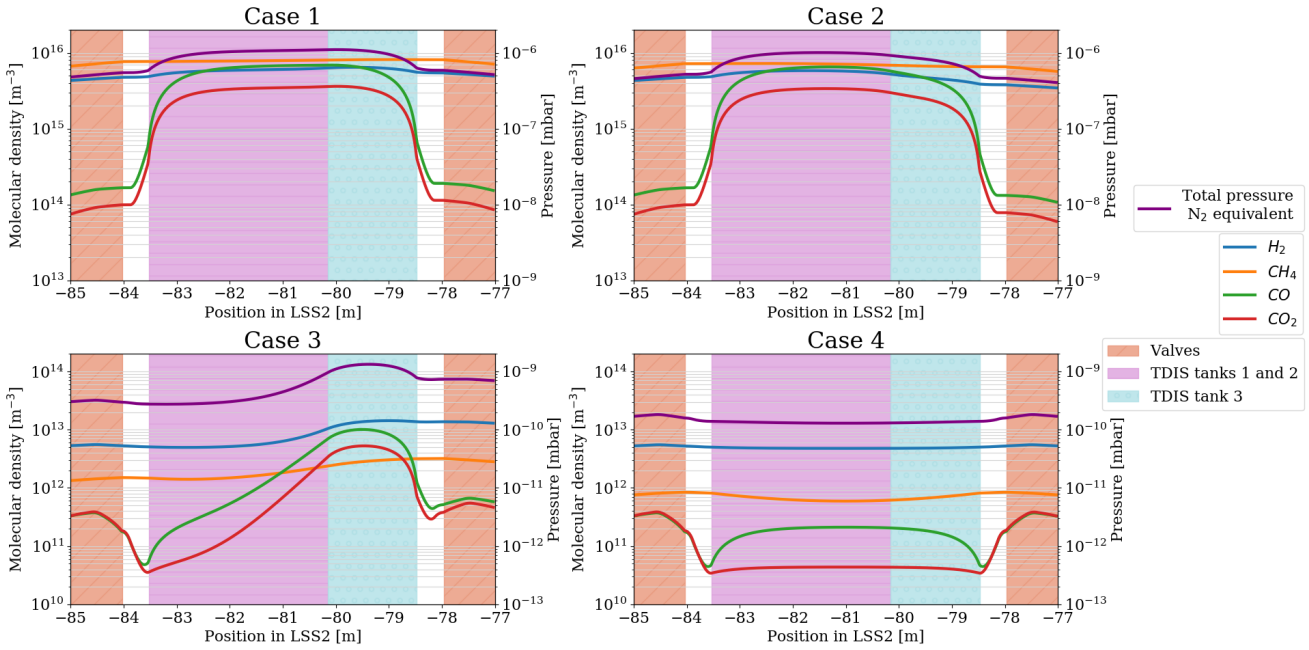

Figure 14: Dynamic density profiles for the different studied cases at a half-gap of 45 mm. The total pressure in N_2 equivalent for a Bayard-Alpert ionization gauge is also shown.

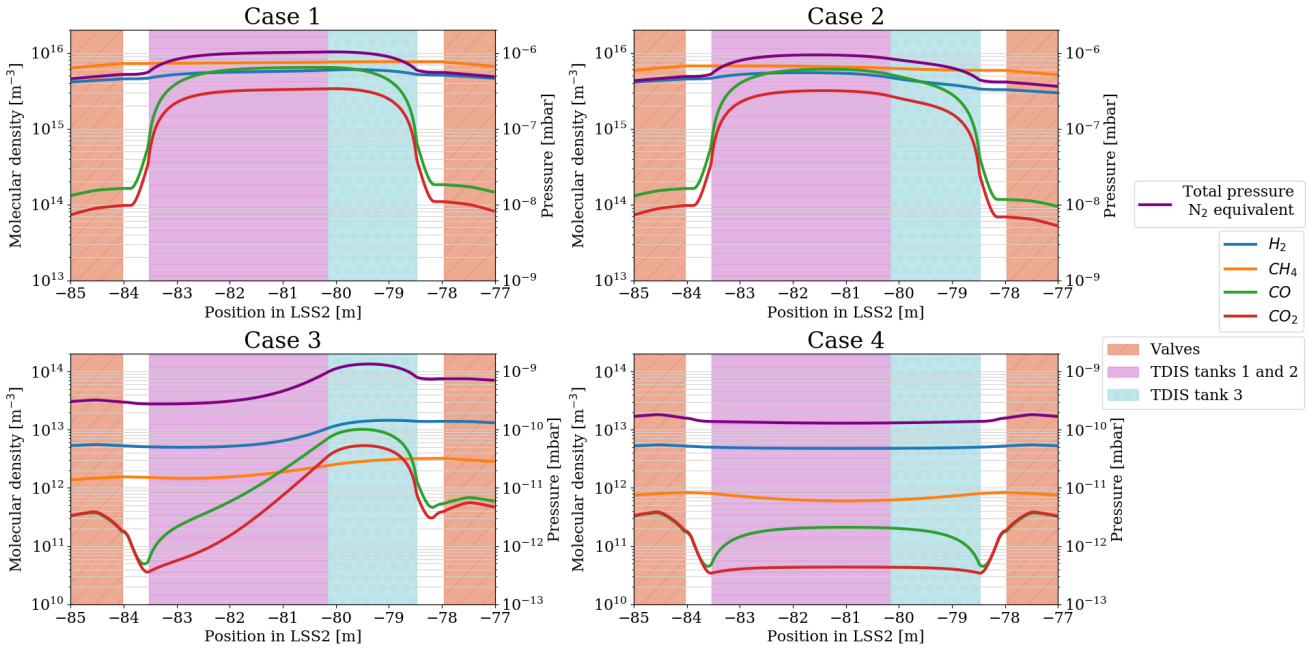

Figure 15: Dynamic density profiles for the different studied cases at a half-gap of 50 mm. The total pressure in N_2 equivalent for a Bayard-Alpert ionization gauge is also shown.

As shown in Fig. 11b, the electron current generated due to the build-up of electron cloud is considerably larger in the third tank of the TDIS than in tanks 1 and 2 for case

1 and 3. In accordance with this result, the dynamic pressure for case 1 and 3 presents a maximum in the region of the third TDIS tank.

In opposition, in case 2 the build-up of electron cloud is larger in the first and second tanks and, as expected, the dynamic pressure profile for this case is dominated by the pressure in the first two tanks.

In case 3 the build-up of electron cloud is effectively suppressed in the first and second tanks of the TDIS due to the applied coatings. The main contribution to electron cloud comes from the third tank for half-gaps larger than 15 mm. Consequently, the maximum dynamic pressure for the case 3 can be found in the region of the third tank of the TDIS for half-gaps larger than 15 mm, and in the saturated NEG chambers before the TDIS tanks for smaller apertures.

In case 4, the electron cloud is effectively suppressed in all the TDIS tanks, and the main contribution to the dynamic pressure comes from the warm modules at both sides of the TDIS. Since the electron flux impinging on the warm modules at both sides of the TDIS is assumed to be constant and independent of the half-gap, the pressure profile for case 4 is expected to remain approximately unchanged for the different half-gaps, with the exception of a slight decrease in the pressure with the increase of the conductance for bigger half-gaps.

Figure 16 shows the dependence of the maximum pressure in the TDIS region as a function of the half-gap, for the different studied cases. The maximum pressure of 1.0×10^{-6} mbar is observed in baseline case 1 and a half-gap of 45 mm.

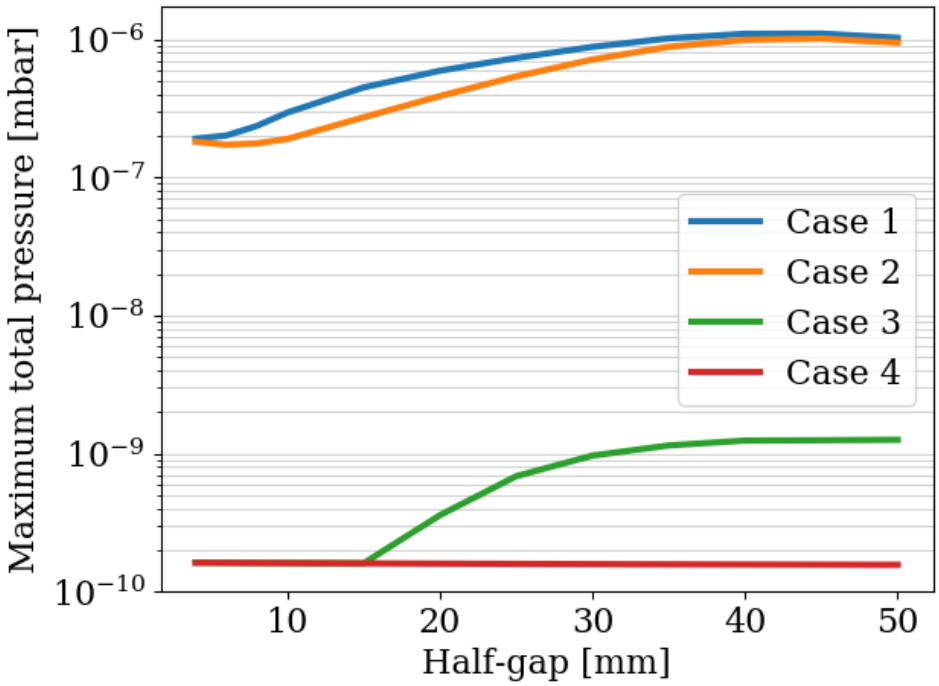

Figure 16: Maximum total pressure rise in N_2 equivalent in a Bayard-Alpert ionization gauge for the different studied cases.

It is interesting to point out that in case 2 the impact of coating only the jaws of the third tank compared to baseline case 1 is small, especially at large half-gaps, with a maximum

reduction of 2×10^{-7} mbar reached for a half-gap of 20 mm.

On the contrary, the effect of coating the RF shield in all three tanks of the TDIS is significant. In case 3, with a-C coating on the RF-shield of the three tanks and uncoated jaws in tank 3, the maximum pressure is not expected to exceed 2×10^{-9} mbar. Finally, if both the jaws of the third tank and the RF-shield of the three tanks are coated (case 4), the maximum dynamic pressure will not exceed a value of 2×10^{-10} mbar, the same as expected in the static vacuum (Fig. 8). In fact, in this last case, it should be emphasized that the maximum pressure rise decreases slightly with the increase in the half-gap due to the increase of the equivalent conductance of the TDIS tanks.

6 Summary and conclusions

In order to estimate the expected vacuum performance of the future TDIS, both static and dynamic pressure profile simulations have been performed using the recently modified, one-dimensional software PyVASCO.

The dynamic pressure simulations presented in this report are mainly focused in the commissioning of the machine after LS2, since it is during this period that the dynamical pressure rise in the TDIS is foreseen to be the highest, and therefore, the most critical for the operation of the machine. However, since estimating precisely the values of the ESD and the SEY in the tanks by the time when high intensity beams start running in the machine is not straightforward, the unrealistic scenario of a short or non-existing conditioning period, immediately followed by nominal beams has been considered.

In order to minimize the error introduced by replacing the highly asymmetric structure of the TDIS tanks by cylinders, a Molflow+ model of this geometry has been implemented. This model has been used to compute the total outgassing area inside the TDIS, the conductance of the equivalent cylinder for different apertures and to estimate the effective pumping speed in the center of the TDIS tanks for the different UHV relevant gases.

The static pressure profile inside the TDIS is dominated by the outgassing of the interior walls, and several measurements and values found in Refs. [9, 10, 13] have been used to estimate the outgassing rate of the different materials that compose the TDIS tanks, adjacent chambers and surrounding valves.

According to earlier results [16] the synchrotron radiation in the TDIS area can be neglected and thus the main contributor to the dynamic pressure rise will be the electron cloud accumulated in the region. Moreover, the new TDIS will be operated at double beam intensities compared to the current TDI, leading to more severe electron cloud formation. For these reasons a special care was taken to compute the electron flux on the surfaces inside the TDIS [12], using the PyECLOUD code. In order to compute the electron cloud profile in the TDIS chambers, two counter rotating beams in the common TDIS chamber have been considered. Due to the bunched structure of both beams, the build-up of electron cloud strongly depends on the time separation of both beams inside the TDIS, but only the total integrated electron current has been considered in this report.

Various coatings of different parts of the geometry are used in order to evaluate their effects on the vacuum performance of the TDIS during operation.

Simulations show that, due to the larger electron current accumulated in tanks 1 and

2, the maximum dynamic pressure in the TDIS reaches a value of 1.0×10^{-6} mbar in the baseline case 1, when the RF-Shield of the two first tanks is not coated. The application of an a-C coating on the jaws of the third tank was found to barely have any impact in case 2.

The application of a-C coatings on the RF-shield of all three tanks can lead to a great improvement in the vacuum performance of the TDIS, causing a decrease of the maximum pressure below 2×10^{-9} mbar, when the jaws of the third tank are left uncoated and below 2×10^{-10} mbar when both the RF-shield in the three tanks and the jaws of the third tank are coated.

Due to the unrealistic conditions considered for the ESD and the SEY in the TDIS chambers in this study, the pressure rise obtained for cases 1 to 3 is foreseen to be considerably smaller than the results presented in this report. However, it is very important to stress out that even under these extreme conditions, cases 3 and 4, with a-C coating, would fulfill immediately the vacuum requirements imposed by the ALICE experiment and the LHC machine.

7 Acknowledgments

Special thanks to Josef Sestak for providing the base Molflow+ model used as input for the simulations, and to Marton Ady for his support in modifying it. Many thanks to Simone Callegari for contributing with the experimental ESD curves used as input in the simulations.

References

[1] G. Apollinari, I. Bjar Alonso, O. Brning, P. Fessia, M. Lamont, L. Rossi, and L. Tavian, "High-Luminosity Large Hadron Collider (HL-LHC) Technical Design Report V. 0.1," tech. rep., 2017. CERN Yellow Reports: Monographs.

[2] P. S. Díaz, "Vacuum layout for the installation of the TDIS," tech. rep., CERN.

[3] SGL Group, *SIGRAFINE R7550*. http://www.sglgroup.com/cms/_common/downloads/products/product-groups/gs/tds/iso/SIGRAFINE_TDS-R7550.02.pdf.

[4] Agilent Technologies, *Agilent Ion Pumps*. https://www.agilent.com/cs/library/catalogs/public/06_Ion_Pumps.pdf.

[5] SAES Group, *CapaciTorr HV Pumps*. https://www.saesgetters.com/sites/default/files/CAPACITORR%20FOLDER.pdf.

[6] A. Rossi, "VASCO (Vacuum Stability COde): multi-gas code to calculate gas density profile in a UHV system," tech. rep., CERN, March 2004.

[7] I. Aichinger, R. Kersevan, and P. Chiggiato, "Analytical methods for vacuum simulations in high energy accelerators for future machines based on LHC performances.," Tech. Rep. arXiv:1707.07525, Jul 2017.

[8] M. Ady, R. Kersevan, and R. Leonid, "Monte Carlo simulations of ultra high vacuum and synchrotron radiation for particle accelerators," May 2016. PhD thesis.

[9] Y. Delaup, "Vacuum test report for LHC Spare TDI n° 1," tech. rep., CERN, 2017. EDMS Document No: 1808397.

[10] G. Cattenoz, "Vacuum test report for LHC Spare TDI n° 2," tech. rep., CERN, 2018. EDMS Document No: 1831835.

[11] J. Sopousek, "Simulation of the LHC dynamic vacuum in presence of synchrotron radiation," tech. rep., CERN, 2016. EDMS 1709714.

[12] G. Skripka and G. Iadarola, "Electron cloud studies for the LHC TDI and HL-LHC TDIS," tech. rep., Aug 2018. CERN-ACC-NOTE-2018-0060.

[13] S. Callegari, "Electron Stimulated Desorption Studies on Copper After Bake-Out in Ultra-High Vacuum and with Different Venting Conditions." Poster presented at EVC15, June 2018.

[14] G. Iadarola, "Electron cloud studies for CERN particle accelerators and simulation code development," March 2014. PhD thesis.

[15] G. Skripka and G. Iadarola, "E-cloud in TDIS." Presented at Electron Cloud Meeting # 53, 2018.

[16] J. Sopousek, "Simulation of dynamic pressure in LHC." CERN, VSC Seminar, July 2016.